

Charmless B decays in modes with similar tree and penguin contributions

IGNACIO BEDIAGA, ON THE BEHALF OF THE LHCb COLLABORATION.

Centro Brasileiro de Pesquisas Físicas, Rio de Janeiro, Brazil

Charmless B decays are dominated by contributions from the short distance amplitudes from tree level and penguin loop-level amplitudes. The Tree contribution presents a weak phase γ . The interference between these two amplitudes can generate a CP asymmetry depending on the relative contribution of each amplitude. In multi-body charmless B decays, these relative contributions can change along the phase space, given a non isotropic distribution of CP asymmetries in the Dalitz plot. Two recent LHCb analyses involving charmless multi-body B decays are discussed: the observation of CP asymmetries in the phase space of the three-body decays $B^\pm \rightarrow \pi^\pm \pi^+ \pi^-$ and $B^\pm \rightarrow \pi^\pm K^+ K^-$; and the angular analysis of the $B^0 \rightarrow \phi K^*(892)^0$ decay.

PRESENTED AT

FPCP-2014- Flavor Physics & CP Violation
Marseille, France, May 25-30, 2014

1 Introduction

Multi-body hadronic B decays have been showing some interesting physics signatures in both; flavor physics and CP violation. The large phase space of charmless B decays together with LHCb high statistics, allows observations of some important distributions related to hadrons interactions. The polarization amplitudes to the $B^0 \rightarrow \phi K^*(892)^0$ decay [1] and the high CP violation observed inside the phase space of the decays $B^\pm \rightarrow \pi^\pm \pi^+ \pi^-$ and $B^\pm \rightarrow \pi^\pm K^+ K^-$ [2] are examples of these new signatures.

The $B^0 \rightarrow \phi K^*(892)^0$ decay involves a spin-0 B-meson decaying into two spin-1 vector mesons. Due to angular momentum conservation there are only three independent configurations of the final-state spin vectors, a longitudinal component where in the B^0 rest frame both resonances are polarized in their direction of motion, and two transverse components with collinear and orthogonal polarizations. Other than measurements of the polarization amplitudes, triple-product asymmetries were studied by LHCb Collaboration [1].

Angular analyses have shown that the longitudinal and transverse components in this decay have roughly equal amplitudes. Similar results are seen in other $B \rightarrow VV$ penguin transitions [3, 4, 5, 6]. The different behavior of tree and penguin decays has attracted much theoretical attention, with several explanations proposed such as large contributions from penguin annihilation effects [8] or final-state interactions [7]. More recent calculations based on QCD factorization [9, 10] are consistent with the data, although with significant uncertainties.

Charmless decays of B mesons to three hadrons are dominated by quasi-two-body processes involving intermediate resonant states. The rich interference pattern present in such decays makes them favorable for the investigation of CP asymmetries that are localized in the phase space [11, 12]. The large samples of charmless B decays collected by the LHCb experiment allow direct CP violation to be measured in regions of phase space. In previous measurements of this type, the phase spaces of $B^\pm \rightarrow K^\pm \pi^+ \pi^-$ and $B^\pm \rightarrow K^\pm K^+ K^-$ decays were observed to have regions of large local asymmetries [2, 13].

Recent efforts have been made to understand the origin of the large asymmetries. For direct CP violation to occur, two interfering amplitudes with different weak and strong phases must be involved in the decay process [14]. Interference between intermediate states of the decay can introduce large strong phase differences, and is one mechanism for explaining local asymmetries in the phase space [15, 16]. Another explanation focuses on final-state $KK \leftrightarrow \pi\pi$ rescattering, which can occur between decay channels with the same flavor quantum numbers [13, 16, 17]. Invariance of CPT symmetry constrains hadron rescattering so that the sum of the partial decay widths, for all channels with the same final-state quantum numbers related by the S matrix, must be equal for charge-conjugated decays. Effects of SU(3) flavor

symmetry breaking have also been investigated and partially explain the observed patterns [16, 18, 19].

The studies reported here are performed using pp collision data, corresponding to an integrated luminosity of 1.0 fb^{-1} , collected at a centre-of-mass energy of 7 MeV with the LHCb detector.

2 $B^0 \rightarrow \phi K^*(892)^0$ signal and the angular fit model

The selection of starts from well reconstructed charged particles with a $p_T > 500 \text{ MeV}$ that traverse the entire spectrometer [20]. Fake tracks, not associated to actual charged particles, are suppressed using the output of a neural network trained to discriminate between these and real particles. To select well-identified pions and kaons, the difference in the logarithms of the likelihood of the kaon hypothesis relative to the pion hypothesis is used. The resulting charged particles are combined to form ϕ and $K^*(892)^0$ meson candidates. The invariant mass of the K^+K^- ($K^+\pi^-$) pair is required to be within $\pm 15 \text{ MeV}/c^2$ ($\pm 150 \text{ MeV}/c^2$) of the known mass of the ϕ ($K^*(892)^0$) meson [21]. Finally, the p_T of the ϕ and $K^*(892)^0$ mesons should both be greater than 900 MeV, and the fit of their two-track vertices should have a $\chi^2 < 9$.

The signal yield is determined from an unbinned maximum likelihood fit to the $K^+K^-K^+\pi^-$ invariant mass distribution. The selected mass range is chosen to avoid modeling partially reconstructed B decays with a missing hadron or photon. In the fit the signal invariant mass distribution is modeled as the sum of a Crystal Ball function [23] and a wider Gaussian function with a common mean. The width and fraction of the Gaussian function are fixed to values obtained using simulated events. A component is also included to account for the small contribution from the decay $B_s^0 \rightarrow \phi K^*(892)^0$ [25]. The shape parameters for this component are in common with the B^0 signal shape and the relative position of the B_s^0 signal with respect to the B^0 signal is fixed using the known mass difference between B_s^0 and B^0 mesons [21]. The invariant mass distribution is shown in Fig. 1, together with the result of the fit, from which a yield of 1655 ± 42 B^0 signal candidates is found. The background is mainly combinatorial and is modeled by an exponential. Possible background from $B^0 \rightarrow \phi\phi$ decays, $B^0 \rightarrow D_s^+K^-$ ($D_s^+ \rightarrow \phi\pi^+$) decays, which would peak in the signal region, is found to be negligible.

An angular analysis is performed with the $B^0 \rightarrow \phi K^*(892)^0$ signal events obtained with the selection above, we performed an angular analysis. The physics parameters of interest for this analysis are defined in Table 1. They include the polarization amplitudes, phases and amplitude differences between B^0 and \bar{B}^0 decays.

The amplitudes and phases can be used to calculate triple-product asymmetries [1]. Non-zero triple-product asymmetries arise either due to a T -violating phase or a CP-conserving phase and final-state interactions. Assuming CPT symmetry, a

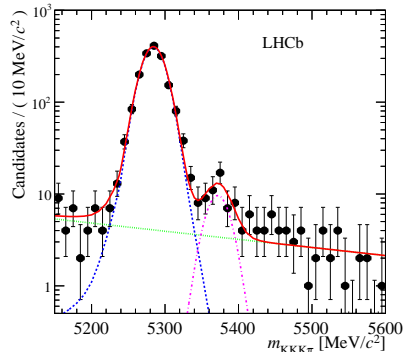


Figure 1: Invariant mass distribution for selected $K^+K^-K^+\pi^-$ candidates. A fit to the model described in the text is superimposed (red solid line). The signal contribution is shown as the blue dotted line. The contribution from combinatorial background is shown in green (dotted line). A contribution from $B_s^0 \rightarrow \phi K^*(892)^0$ (purple dot-dashed line) decays is visible around the known B_s^0 meson mass.

T -violating phase, which is a *true* asymmetry, implies that CP is violated. Otherwise *fake* asymmetry indicate CP conservation and the presence of final state interaction [24].

The acceptance of the detector is not uniform as a function of the decay angle of the $K^+\pi^-$ system (θ_1) and the $K^+\pi^-$ invariant mass. This acceptance is modelled using a four-dimensional function that depends on the three decay angles and the $K^+\pi^-$ invariant mass. The shape of this function is obtained from simulated data.

3 Results

The fit function incorporate other than the P-wave contribution, for the first time the S-wave component is include in this kind of study. The differential decay width depends on the invariant masses of the $K^+\pi^-$ and K^+K^- systems, denoted $m_{K\pi}$ and m_{KK} , respectively. The P-wave $K^+\pi^-$ amplitude is parameterized using a relativistic spin-1 Breit-Wigner resonance function. The P-wave K^+K^- amplitude is modeled in a similar way using the values $m_0(\phi) = 1019.455$ MeV and $\Gamma_0(\phi) = 4.26$ MeV [21]. The S-wave contributions in both the K^+K^- and $K^+\pi^-$ system are considered. The default fit uses the LASS parameterization to model the $K^+\pi^-$ S-wave [22]. As variations of this, both a pure phase-space model and a spin-0 relativistic Breit-Wigner with mean and width of the $K_0^*(1430)$ resonance are considered [21]. For the K^+K^- S-wave a pure phase-space model is tried in place of the Flatté parameterization [26]. The largest observed deviation from the nominal fit is taken as a systematic uncertainty [1].

Figure 2 shows the data distributions for the intermediate resonance masses and helicity angles with the projections of the best fit overlaid. The goodness of fit is estimated using a point-to-point dissimilarity test [27], the corresponding p -value is 0.64.

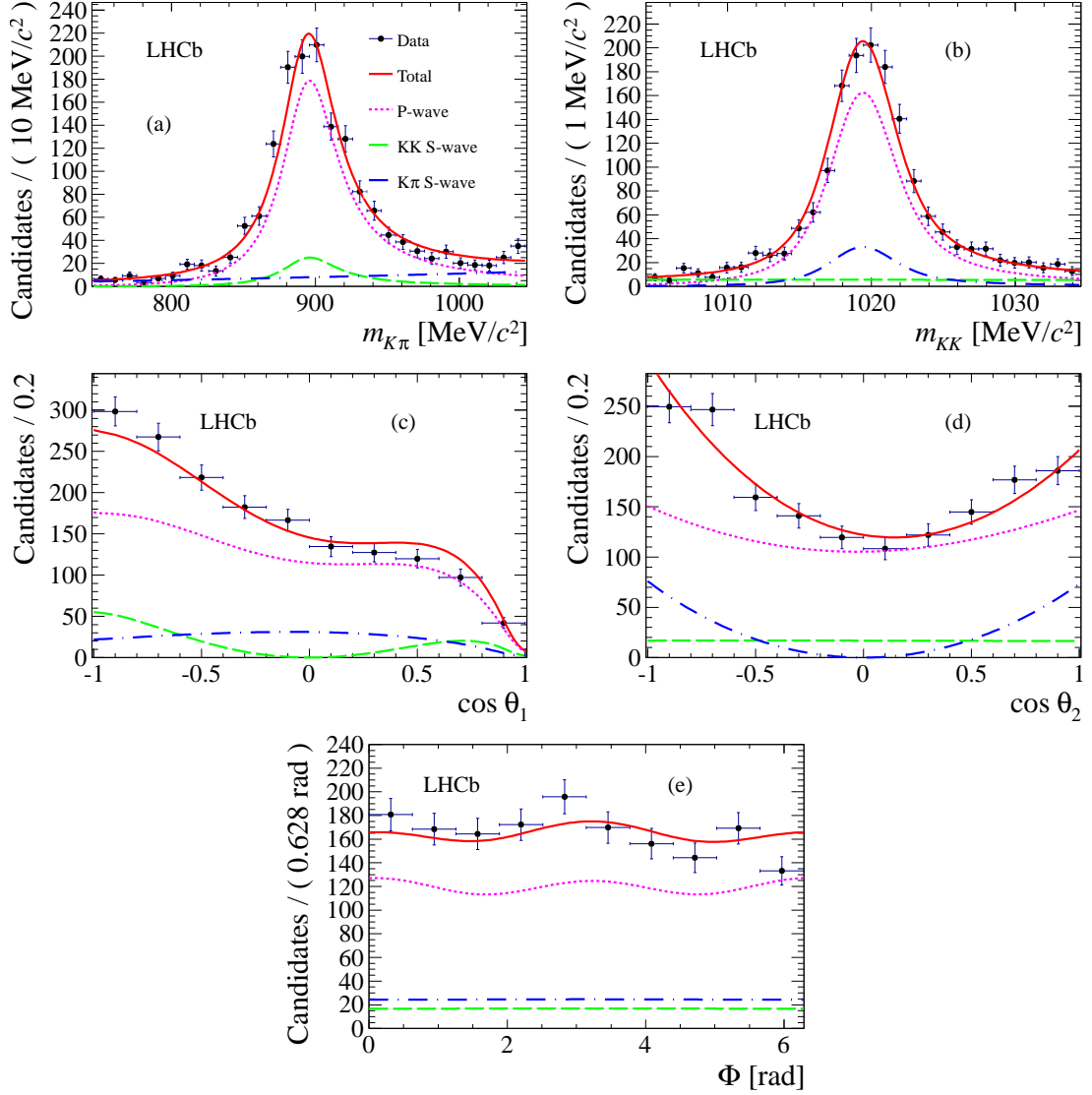


Figure 2: Data distributions for the helicity angles and of the intermediate resonance masses: (a) $m_{K\pi}$ and (b) m_{KK} , (c) $\cos \theta_1$, (d) $\cos \theta_2$ and (e) Φ . The background has been subtracted using the SPlot technique. The results of the fit are superimposed.

The fit results are listed in Table 1. The longitudinal distribution f_L , defined in [1], returned by the fit is close to 0.5, indicating that the longitudinal and transverse

polarizations (f_{\perp}), have similar size. Significant S-wave contributions are found in both the $K^+\pi^-$ and K^+K^- systems. The CP asymmetries in both the amplitudes and the phases are consistent with zero.

The largest systematic uncertainties on the results of the angular analysis arise from the understanding of the detector acceptance. The angular acceptance function is determined from simulated events. This and other systematic uncertainties are discussed in Ref. [1].

Table 1: Angular analysis results. The parameters are defined in Ref. [1] . The first and second uncertainties are statistical and systematic, respectively.

Parameter	Definition	Fitted value
f_L	$0.5(A_0 ^2/F_P + \bar{A}_0 ^2/\bar{F}_P)$	$0.497 \pm 0.019 \pm 0.015$
f_{\perp}	$0.5(A_{\perp} ^2/F_P + \bar{A}_{\perp} ^2/\bar{F}_P)$	$0.221 \pm 0.016 \pm 0.013$
$f_S(K\pi)$	$0.5(A_S^{K\pi} ^2 + \bar{A}_S^{K\pi} ^2)$	$0.143 \pm 0.013 \pm 0.012$
$f_S(KK)$	$0.5(A_S^{KK} ^2 + \bar{A}_S^{KK} ^2)$	$0.122 \pm 0.013 \pm 0.008$
δ_{\perp}	$0.5(\arg A_{\perp} + \arg \bar{A}_{\perp})$	$2.633 \pm 0.062 \pm 0.037$
δ_{\parallel}	$0.5(\arg A_{\parallel} + \arg \bar{A}_{\parallel})$	$2.562 \pm 0.069 \pm 0.040$
$\delta_S(K\pi)$	$0.5(\arg A_S^{K\pi} + \arg \bar{A}_S^{K\pi})$	$2.222 \pm 0.063 \pm 0.081$
$\delta_S(KK)$	$0.5(\arg A_S^{KK} + \arg \bar{A}_S^{KK})$	$2.481 \pm 0.072 \pm 0.048$
\mathcal{A}_0^{CP}	$(A_0 ^2/F_P - \bar{A}_0 ^2/\bar{F}_P)/(A_0 ^2/F_P + \bar{A}_0 ^2/\bar{F}_P)$	$-0.003 \pm 0.038 \pm 0.005$
\mathcal{A}_{\perp}^{CP}	$(A_{\perp} ^2/F_P - \bar{A}_{\perp} ^2/\bar{F}_P)/(A_{\perp} ^2/F_P + \bar{A}_{\perp} ^2/\bar{F}_P)$	$+0.047 \pm 0.074 \pm 0.009$
$\mathcal{A}_S(K\pi)^{CP}$	$(A_S^{K\pi} ^2 - \bar{A}_S^{K\pi} ^2)/(A_S^{K\pi} ^2 + \bar{A}_S^{K\pi} ^2)$	$+0.073 \pm 0.091 \pm 0.035$
$\mathcal{A}_S(KK)^{CP}$	$(A_S^{KK} ^2 - \bar{A}_S^{KK} ^2)/(A_S^{KK} ^2 + \bar{A}_S^{KK} ^2)$	$-0.209 \pm 0.105 \pm 0.012$
δ_{\perp}^{CP}	$0.5(\arg A_{\perp} - \arg \bar{A}_{\perp})$	$+0.062 \pm 0.062 \pm 0.005$
δ_{\parallel}^{CP}	$0.5(\arg A_{\parallel} - \arg \bar{A}_{\parallel})$	$+0.045 \pm 0.069 \pm 0.015$
$\delta_S(K\pi)^{CP}$	$0.5(\arg A_S^{K\pi} - \arg \bar{A}_S^{K\pi})$	$+0.062 \pm 0.062 \pm 0.022$
$\delta_S(KK)^{CP}$	$0.5(\arg A_S^{KK} - \arg \bar{A}_S^{KK})$	$+0.022 \pm 0.072 \pm 0.004$

The results for the P-wave parameters are consistent with, but more precise than previous measurements. All measurements are consistent with the presence of a large transverse component rather than the naive expectation of a dominant longitudinal polarization. It is more difficult to make comparisons for the S-wave components as this is the first measurement to include consistently the effect of the S-wave in the K^+K^- system, and because the $K^+\pi^-$ mass range is different with respect to the range used in previous analyses.

The values for the triple-product asymmetries are derived from the measured parameters and given in Table 2. The true asymmetries are consistent with zero,

showing no evidence for physics beyond the Standard Model. In contrast, all but one of the fake asymmetries are significantly different from zero, indicating the presence of final-state interactions.

Table 2: Triple-product asymmetries. The first and second uncertainties on the measured values are statistical and systematic, respectively.

Asymmetry	Measured value
$A_T^1(\text{true})$	$-0.007 \pm 0.012 \pm 0.002$
$A_T^2(\text{true})$	$+0.004 \pm 0.014 \pm 0.002$
$A_T^3(\text{true})$	$+0.004 \pm 0.006 \pm 0.001$
$A_T^4(\text{true})$	$+0.002 \pm 0.006 \pm 0.001$
$A_T^1(\text{fake})$	$-0.105 \pm 0.012 \pm 0.006$
$A_T^2(\text{fake})$	$-0.017 \pm 0.014 \pm 0.003$
$A_T^3(\text{fake})$	$-0.063 \pm 0.006 \pm 0.005$
$A_T^4(\text{fake})$	$-0.019 \pm 0.006 \pm 0.007$

4 $B^\pm \rightarrow \pi^\pm K^+ K^-$ and $B^\pm \rightarrow \pi^\pm \pi^+ \pi^-$ inclusive CP asymmetries

The inclusive CP asymmetries involves the difference of total number of events of the negative and positive B^\pm three body decays divided by the sum of them. For these decays are required to satisfy a set of selection criteria related with their transverse momenta, vertex and tracking quality. Final-state kaons and pions are further selected using particle identification information, provided by two ring-imaging Cherenkov detectors [28], and are required to be incompatible with a muon [29]. The kinematic selection is common to both decay channels, while the particle identification selection are specific to each final state. Charm contributions are removed by excluding the regions of ± 30 MeV around the world average value of the D^0 mass [21] in the two-body invariant masses $m_{\pi\pi}$, $m_{K\pi}$ and m_{KK} .

Unbinned extended maximum likelihood fits to the mass spectra of the selected B^\pm candidates are performed to obtain the signal yields and raw asymmetries. Both signals components are parametrized by a Cruijff function [30] with equal left and right widths and different radiative tails to account for the asymmetric effect of final-state radiation on the signal shape. The means and widths are allowed to vary freely in the fit, while the tail parameters are fixed to the values obtained from simulation. The combinatorial background is described by an exponential distribution whose parameter is left free in the fit. The backgrounds due to partially reconstructed four-body B decays are parametrized by an ARGUS distribution [31] convolved with a

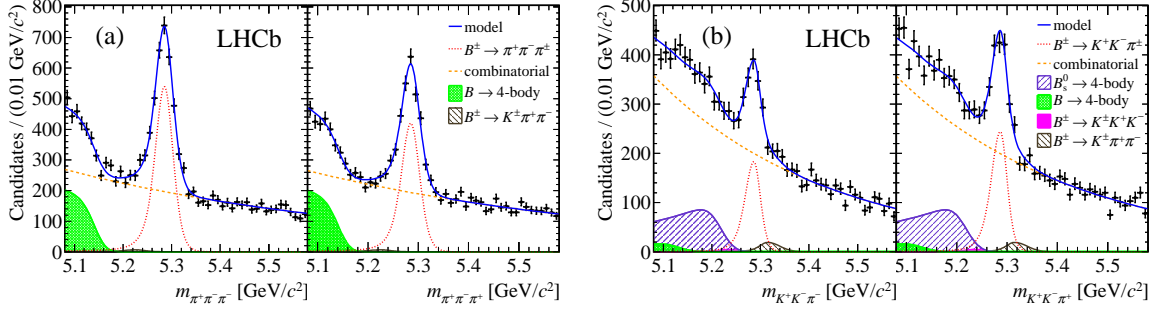


Figure 3: Invariant mass spectra of (a) $\pi^\pm\pi^+\pi^-$ decays and (b) $\pi^\pm K^+K^-$ decays. The left panel in each figure shows the B^- modes and the right panel shows the B^+ modes. The results of the unbinned maximum likelihood fits are overlaid. The main components of the fit are also shown.

Gaussian resolution function. For the $\pi^\pm\pi^+\pi^-$ modes the shape and yield parameters describing the backgrounds are varied in the fit, while for $\pi^\pm K^+K^-$ decays they are taken from simulation, due to a further contribution from four-body B_s . Peaking background are defined as three-body B decays modes. The shapes and yields of the peaking backgrounds are obtained from simulation. The invariant mass spectra of the $\pi^\pm K^+K^-$ and $\pi^\pm\pi^+\pi^-$ candidates are shown in Fig. 3.

The signal yields obtained are $N(KK\pi) = 1870 \pm 133$ and $N(\pi\pi\pi) = 4904 \pm 148$, and the raw asymmetries are $A_{raw}(KK\pi) = -0.143 \pm 0.040$ and $A_{raw}(\pi\pi\pi) = 0.124 \pm 0.021$, where the uncertainties are statistical. The CP asymmetries are expressed in terms of the measured raw asymmetries, corrected for effects induced by the detector acceptance and interactions of final-state pions with matter, as well as for a possible B -meson production asymmetry. To take care of these effects we use these informations from the control channel $B^\pm \rightarrow J/\Psi K^\pm$ with $J/\Psi \rightarrow \mu\mu^-$.

The methods used in estimating the systematic uncertainties of the signal model, combinatorial background, peaking background, and acceptance correction are the same as those used in Ref. [13]. For $\pi^\pm K^+K^-$ decays, we also evaluate a systematic uncertainty due to the partially reconstructed background model by varying the mean and resolution according to the difference between simulation and data obtained from the signal component. The complete list of systematic and uncertainties can be obtained in Ref. [2].

The results obtained for the inclusive CP asymmetries of the $B^\pm \rightarrow \pi^\pm K^+K^-$ and $B^\pm \rightarrow \pi^\pm\pi^+\pi^-$ decays are

$$A_{CP}(B^\pm \rightarrow \pi^\pm K^+K^-) = -0.141 \pm 0.040 \pm 0.018 \pm 0.007,$$

$$A_{CP}(B^\pm \rightarrow \pi^\pm\pi^+\pi^-) = 0.117 \pm 0.021 \pm 0.009 \pm 0.007,$$

where the first uncertainty is statistical, the second is the experimental systematic,

and the third is due to the CP asymmetry of the control channel $B^\pm \rightarrow J/\Psi K^\pm$ reference mode [21].

5 CP asymmetry distribution in Dalitz phase space

In addition to the inclusive charge asymmetries, we study the asymmetry distributions in the two-dimensional phase space of two-body invariant masses [2]. The Dalitz plot distributions in the signal region are divided into bins with approximately equal numbers of events in the combined B^- and B^+ samples. Figure 4 shows the raw asymmetries (not corrected for efficiency), computed using the number of negative (N^-) and positive (N^+) entries in each bin of the $B^\pm \rightarrow \pi^\pm K^+ K^-$ and $B^\pm \rightarrow \pi^\pm \pi^+ \pi^-$ Dalitz plots. The $B^\pm \rightarrow \pi^\pm \pi^+ \pi^-$ Dalitz plot is symmetrized.

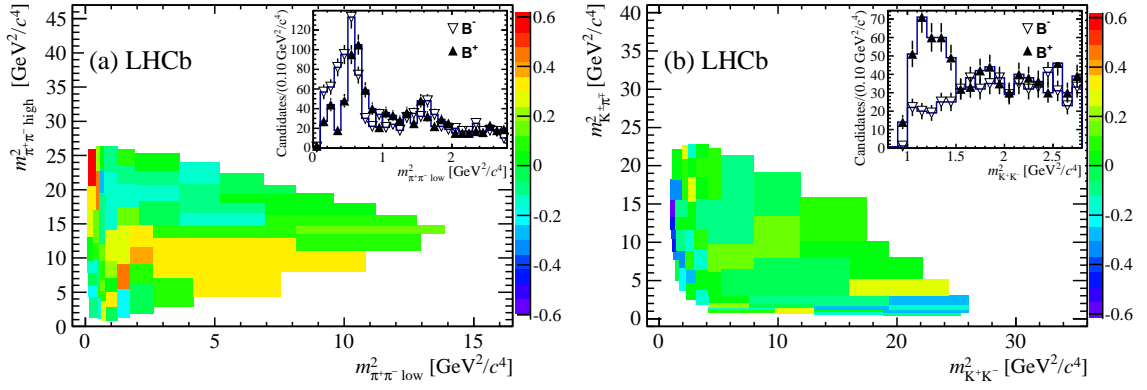


Figure 4: Asymmetries of the number of events (including signal and background) in bins of the Dalitz plot, for (a) $B^\pm \rightarrow \pi^\pm \pi^+ \pi^-$ and (b) $B^\pm \rightarrow \pi^\pm K^+ K^-$ decays. The inset figures show the projections of the number of events in bins of (a) the variable $M_{high}^2(\pi\pi) > 15$ and (b) the variable $M^2(KK)$. The distributions are not corrected for efficiency.

The CP asymmetries are further studied in the regions where large raw asymmetries are found. The regions are defined as $M_{high}^2(\pi\pi) > 15$ and $M_{low}^2(\pi\pi) < 0.4 \text{ GeV}^2$ for the $B^\pm \rightarrow \pi^\pm \pi^+ \pi^-$ mode, and $M^2(KK) < 1.5 \text{ GeV}^2$ for the $B^\pm \rightarrow \pi^\pm K^+ K^-$ mode. Unbinned extended maximum likelihood fits are performed to the mass spectra of the candidates in these regions, using the same models as for the global fits. The spectra are shown in Fig. 5. The resulting signal yields and raw asymmetries for the two regions are $N^{\text{reg}}(KK\pi) = 342 \pm 28$ and $A_{\text{raw}}^{\text{reg}}(KK\pi) = -0.658 \pm 0.070$ for the $B^\pm \rightarrow \pi^\pm K^+ K^-$ mode, and $N^{\text{reg}}(\pi\pi\pi) = 229 \pm 20$ and $A_{\text{raw}}^{\text{reg}}(\pi\pi\pi) = 0.555 \pm 0.082$ for the $B^\pm \rightarrow \pi^\pm \pi^+ \pi^-$ mode. The CP asymmetries are obtained from the raw asymmetries applying an acceptance correction, like above to the inclusive measurement.

The final results and the systematic uncertainties are produced in a similar way that the ones of the inclusive CP asymmetries and are presented in Ref. [2]

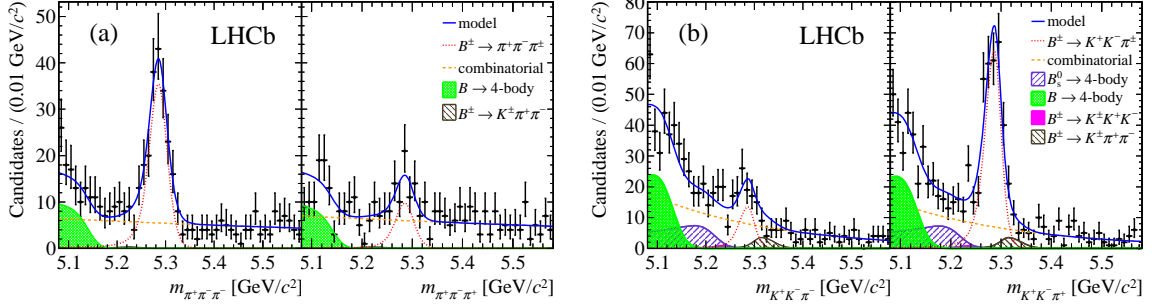


Figure 5: Invariant mass spectra of (a) $B^\pm \rightarrow \pi^\pm \pi^+ \pi^-$ decays in the region $M_{high}^2(\pi\pi) > 15$ and $M_{low}^2(\pi\pi) < 0.4 \text{ GeV}^2$, and (b) $B^\pm \rightarrow \pi^\pm K^+ K^-$ decays in the $M^2(KK) < 1.5 \text{ GeV}^2$ region. The left panel in each figure shows the B^- modes and the right panel shows the B^+ modes. The results of the unbinned maximum likelihood fits are overlaid.

These charge asymmetries are not uniformly distributed in the phase space. For $B^\pm \rightarrow \pi^\pm K^+ K^-$ decays, where no significant resonant contribution is expected, we observe a very large negative asymmetry concentrated in a restricted region of the phase space in the low $K^+ K^-$ invariant mass. For $B^\pm \rightarrow \pi^\pm \pi^+ \pi^-$ decays, a large positive asymmetry is measured in the low $M_{low}^2(\pi\pi)$ and high $M_{high}^2(\pi\pi)$ phase-space region, not clearly associated to a resonant state. The evidence presented here for CP violation in $B^\pm \rightarrow \pi^\pm K^+ K^-$ and $B^\pm \rightarrow \pi^\pm \pi^+ \pi^-$ decays, along with the recent evidence for CP violation in $B^\pm \rightarrow K^\pm \pi^+ \pi^-$ and $B^\pm \rightarrow K^\pm K^+ K^-$ decays [13] and recent theoretical developments [16, 17, 18, 15], indicate new mechanisms for CP asymmetries, which should be incorporated in models for future amplitude analyses of charmless three-body B decays.

References

- [1] LHCb collaboration, R. Aaij *et al.*, JHEP **1405** (2014) 069.
- [2] LHCb collaboration, R. Aaij *et al.*, Phys. Rev. Lett. **112** (2014) 1, 011801
- [3] BaBar collaboration, P. del Amo Sanchez *et al.*, Phys. Rev. **D83** (2011) 051101.
- [4] Belle collaboration, J. Zhang *et al.*, Phys. Rev. Lett. **95** (2005) 141801.
- [5] BaBar collaboration, B. Aubert *et al.*, Phys. Rev. Lett. **97** (2006) 201801.

- [6] LHCb collaboration, R. Aaij *et al.*, Phys. Lett. **B709** (2012) 50.
- [7] A. Datta *et al.*, Phys. Rev. **D76** (2007) 034015.
- [8] A. L. Kagan, Phys. Lett. **B601** (2004) 151.
- [9] M. Beneke, J. Rohrer, and D. Yang, Nucl. Phys. **B774** (2007) 64.
- [10] H.-Y. Cheng and C.-K. Chua, Phys. Rev. **D80** (2009) 114026.
- [11] I. Bediaga *et al.*, Phys. Rev. **D80** (2009) 096006.
- [12] I. Bediaga *et al.*, Phys. Rev. **D86** (2012) 036005.
- [13] LHCb collaboration, R. Aaij Phys. Rev. Lett. **111** (2013) 101801.
- [14] M. Bander, D. Silverman, and A. Soni, Phys. Rev. Lett. **43** (1979) 242.
- [15] Z.-H. Zhang, X.-H. Guo, and Y.-D. Yang, Phys. Rev. **D87** (2013) 076007.
- [16] B. Bhattacharya, M. Gronau, and J. L. Rosner, Phys. Lett. **B726** (2013) 337.
- [17] I. Bediaga, O. Lourenço and T. Frederico, Phys. Rev. **D89** (2014) 094013.
- [18] D. Xu, G.-N. Li, and X.-G. He, Int. J. Mod. Phys. **A29** (2014) 1450011.
- [19] M. Gronau, Phys. Lett. **B727** (2013) 136.
- [20] LHCb collaboration, R. Aaij *et al.*, Phys. Rev. **D87** (2013) 112012.
- [21] Particle Data Group, J. Beringer *et al.*, Phys. Rev. **D86** (2012) 010001
- [22] LASS collaboration, D. Aston *et al.*, Nucl. Phys. **B296** (1988) 493
- [23] T. Skwarnicki, *A study of the radiative cascade transitions between the Upsilon-prime and Upsilon resonances*, PhD thesis, Institute of Nuclear Physics, Krakow, 1986, <http://inspirehep.net/record/230779/files/230779.pdf> DESY-F31-86-02.
- [24] M. Gronau and J. L. Rosner, Phys. Rev. **D84** (2011) 096013
- [25] LHCb collaboration, R. Aaij *et al.*, JHEP **11** (2013) 092.
- [26] S. Flatté, Phys. Lett. **B63** (1976) 224
- [27] M. Williams, JINST **5** (2010) P09004.
- [28] M. Adinolfi *et al.*, Eur. Phys. J. **C73** (2013) 2431.

- [29] Archilli *et al.*, *Performance of the muon identification at LHCb*, *JINST* **8** (2013) P10020.
- [30] BaBar collaboration, P. del Amo Sanchez *et al.*, *Phys. Rev.* **D82** (2010) 051101.
- [31] ARGUS collaboration, H. Albrecht *et al.*, *Phys. Lett.* **B229** (1989) 304.